ATLAS PUB Note

ATL-PHYS-PUB-2019-009

23rd March 2019

Constraint of the Higgs boson self-coupling from Higgs boson differential production and decay measurements

The ATLAS Collaboration

This note sets constraints on the Higgs boson self-coupling exploiting single Higgs boson production. The Higgs boson cross sections, the branching fractions and the Higgs boson kinematics are affected by the Higgs-boson self coupling contribution through next to leading order electroweak corrections. The constraints are obtained by combining the data of the analyses targeting the $\gamma\gamma$, ZZ^*, WW^*, $\tau\tau$ and $b\bar{b}$ decay channels, collected at $\sqrt{s} = 13$ TeV, corresponding to an integrated luminosity of up to 80 fb^{-1}. With the assumption that new physics affects only the Higgs boson self-coupling (λ_{HHH}), the ratio $\lambda_{HHH}/\lambda_{HHH}^{\mathrm{SM}}$ is determined to be $\lambda_{HHH}/\lambda_{HHH}^{\mathrm{SM}} = 4.0^{+4.3}_{-4.1}$, excluding values outside the interval $-3.2 < \lambda_{HHH}/\lambda_{HHH}^{\mathrm{SM}} < 11.9$ at the 95% C.L. Results with less stringent assumptions are also provided.

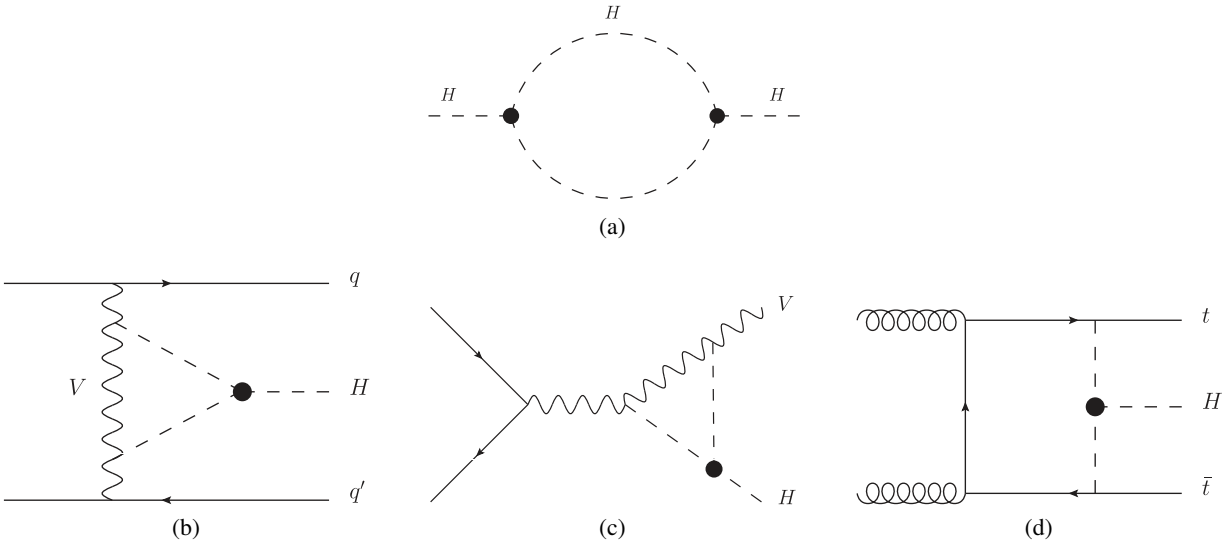

Figure 1: Examples of one loop λ_{HHH}-dependent diagrams for the Higgs boson self energy (a) and the single Higgs boson production in the VBF (b), VH (c), and $t\bar{t}H$ (d) modes. The self-coupling vertex is indicated by the filled circle.

1 Introduction

After the discovery of the Higgs boson by the ATLAS [1] and CMS [2] experiments, the properties of this new particle have been probed by the two experiments, testing their compatibility with the prediction of the Standard Model (SM). During the two runs of data-taking of the Large Hadron Collider (LHC) at CERN, the Higgs production cross-sections and decay branching ratios in various channels have been measured with an increasing precision, as well as the Higgs boson couplings with the SM particles [3–5]. Nevertheless the properties of the Higgs scalar potential, and in particular the Higgs boson self-coupling, are still largely unconstrained. The most recent constraints on the Higgs boson trilinear self-coupling, λ_{HHH}, have been set in the context of a direct search of double Higgs boson production. Results are reported in terms of $\kappa_\lambda = \lambda_{HHH}/\lambda^{SM}_{HHH}$, which is the ratio of the Higgs boson self-coupling to its SM expectation. It is constrained to at 95% confidence level (C.L.) to $-5.0 < \kappa_\lambda < 12.1$ [6] and $-11.8 < \kappa_\lambda < 18.8$ [7] by ATLAS and CMS, respectively, using up to 36 fb^{-1}of Run-2 data.

An alternative and complementary approach to study the Higgs boson self-coupling has been proposed in the Refs. [8–13]. Single Higgs processes do not depend on λ_{HHH} at leading order (LO), but the Higgs trilinear self-coupling contributions need to be taken into account for the calculation of the complete next-to-leading (NLO) electro-weak (EW) corrections. In particular, λ_{HHH} contributes at NLO EW via Higgs self energy loop corrections and additional diagrams, as shown by the examples in Figure 1. Therefore, an indirect constraint on λ_{HHH} can be extracted by comparing precise measurements of single Higgs production yields and the SM predictions corrected for the λ_{HHH}-dependent NLO EW effects. Refs. [8, 9] propose a framework for a global fit to constrain the Higgs trilinear coupling, where all the Higgs boson production and decay channels are modified by parameters:

$$\mu_{if}(\kappa_\lambda) = \mu_i(\kappa_\lambda) \times \mu_f(\kappa_\lambda) \equiv \frac{\sigma_i(\kappa_\lambda)}{\sigma_{\mathrm{SM},i}} \times \frac{\mathrm{BR}_f(\kappa_\lambda)}{\mathrm{BR}_{\mathrm{SM},f}}\,, \tag{1}$$

where μ_i and μ_f describe respectively the multiplicative corrections of the expected SM Higgs production cross-sections ($\sigma_{\mathrm{SM},i}$) and each decay channel branching fraction ($\mathrm{BR}_{\mathrm{SM},f}$) as a function of the anomalous values of the trilinear Higgs self-coupling κ_λ. The functional dependence of $\mu_i(\kappa_\lambda)$ and $\mu_f(\kappa_\lambda)$ on κ_λ varies according to the production mode and the decay channel. Moreover, these functions depend on the kinematic region considered within each process, especially for the VH and $t\bar{t}H$ production modes. In this work, the differential distributions of the VBF, WH and ZH production modes are exploited to constrain κ_λ by using the cross-section measurements in regions defined within the simplified template cross-section (STXS) framework [14, 15].

The note describes a global fit of κ_λ based on the combined measurements of single Higgs production and decay rates [4]. They include analyses targeting the $H \to \gamma\gamma$ [16–18], $H \to ZZ^*$ [19, 20] , VH, $H \to b\bar{b}$ [21, 22], $H \to WW^*$ [23], and $H \to \tau\tau$ [24] decay channels, as well as two analyses targeting Higgs boson associated production with a top–antitop pair, in $b\bar{b}$ and multileptons final states [25, 26]. The results presented are obtained using data collected at $\sqrt{s} = 13$ TeV with an integrated luminosity ranging from 36.1 fb^{-1}to 79.1 fb^{-1}.

The note is organized as follows: Section 2 reviews the dataset and input measurements, Section 3 summarises briefly the theoretical framework, Section 4 discusses the statistical model, Section 5 presents the results of the fit, and Section 6 provides a summary.

2 Data and input measurement

The results shown in this note are based on data collected by the ATLAS experiment [27, 28] in 2015, 2016 and 2017. The integrated luminosities for the analysed Higgs boson decay channels are summarised in Table 1. Details about the individual analyses can be found in the references reported in the same table. Each analysis separates the selected events into orthogonal kinematic and topological regions, called

Table 1: Integrated luminosity of the dataset used for each input analysis to the combination. The last column provides references to publications describing each analysis in detail.

Analysis	Integrated luminosity (fb^{-1})	Ref.
$H \to \gamma\gamma$ (including $t\bar{t}H$, $H \to \gamma\gamma$)	79.8	[16–18]
$H \to ZZ^* \to 4\ell$ (including $t\bar{t}H$, $H \to ZZ^* \to 4\ell$)	79.8	[19, 20]
$H \to WW^* \to e\nu\mu\nu$	36.1	[23]
$H \to \tau\tau$	36.1	[24]
VH, $H \to b\bar{b}$	79.8	[21, 22]
$t\bar{t}H$, $H \to b\bar{b}$ and $t\bar{t}H$ multilepton	36.1	[25, 26]

categories, that are summarized in Table 2.

The categories, defined according to the reconstructed final state, are designed to maximize the sensitivity to each truth-level region defined within the simplified template cross-section framework [14, 15]. In particular, they are based on the stage-1 of the STXS framework within which, depending on Higgs boson production mode, the phase space is subdivided as follows:

- the gluon-fusion production mode is subdivided in regions of jet multiplicity and transverse momentum of the Higgs boson, p_{T}^{H}. Additionally, two regions with VBF-like kinematics, defined by the presence of two jets with large dijet mass, are also considered. The $b\bar{b}H$ and $gg \to Z(had)H$ production modes are considered as small additional contributions to the expected yield in these regions;
- quark-initiated production processes $qq \to Hqq$ are split into a region with a high-$\mathrm{p_T}$ jet, two VBF-like regions, a region with two jets consistent with $V(\to qq)H$ production, and a region for the remaining events;
- leptonic decays of the vector boson in VH and $gg \to ZH$ production modes are split into $qq \to H\ell\nu$, $qq \to H\ell\ell$ and $qq \to H\nu\nu$ final states, and further split as a function of the vector-boson transverse momentum $\mathrm{p}_{\mathrm{T}}^{V}$;
- the $t\bar{t}H$ and tH production modes are considered inclusively in one single region.

Table 2: Summary of the signal categories entering the combined measurements. Each 0-jet and 1-jet $H \to WW^*$ entry is subdivided into two categories depending on the leading lepton flavour being either e or μ. For $H \to \tau\tau$, each entry corresponds to 3 categories for $\tau_{\text{lep}}\tau_{\text{lep}}$ (leptonic decay of both τ's), $\tau_{\text{lep}}\tau_{\text{had}}$ (one τ decays leptonically and one τ decays hadronically) and $\tau_{\text{had}}\tau_{\text{had}}$ (both τ's decay hadronically), unless otherwise specified. For the $t\bar{t}H$ production, "multilepton" refers to decays of the Higgs boson with one or more leptons, and encompasses $H \to WW^*$, $H \to \tau\tau$, and $H \to ZZ^*$ excluding $H \to ZZ^* \to 4\ell$, "hadronic" refers to the full hadronic decay of the $t\bar{t}$ system, "leptonic" refers to the case where the $t\bar{t}$ decay products contain at least one lepton, "boosted" when the H decaying to $b\bar{b}$ is reconstructed as a fat jet, "resolved" when both $\Delta R = 0.4$ jets are reconstructed, 1 ℓ and 2 ℓ when there is exactly 1 lepton and 2 leptons in the final state, respectively. In the table ℓ refers to e or μ, ℓ_2 to the lepton of lowest p_{T}, $E_{\text{T}}^{\text{miss}}$ to the missing transverse energy, j to a light jet, $j1$ to the light jet of highest p_{T}; $p_{\text{T}}^{\ell+E_{\text{T}}^{\text{miss}}}$ is the p_{T} of the $\ell, E_{\text{T}}^{\text{miss}}$ system, $p_{\text{T}}^{4\ell}$ the p_{T} of the four lepton system and similarly for $p_{\text{T}}^{\gamma\gamma}$, $p_{\text{T}}^{\tau\tau}$ and $p_{\text{T}}^{\gamma\gamma jj}$. p_{T}^{V} refers to the p_{T} of the vector boson (V) in the VH category, $m_{\ell\ell}$ is the invariant mass of the di-lepton system.

	$H \to \gamma\gamma$	$H \to ZZ^*$	$H \to WW^*$	$H \to \tau\tau$	$H \to b\bar{b}$
$t\bar{t}H$	$t\bar{t}H$ leptonic (3 categories) $t\bar{t}H$ hadronic (4 categories)	$t\bar{t}H$ multilepton 1 ℓ + 2 τ_{had} $t\bar{t}H$ multilepton 2 opposite-sign ℓ + 1 τ_{had} $t\bar{t}H$ multilepton 2 same-sign ℓ (categories for 0 or 1 τ_{had}) $t\bar{t}H$ multilepton 3 ℓ (categories for 0 or 1 τ_{had}) $t\bar{t}H$ multilepton 4 ℓ (except $H \to ZZ^* \to 4\ell$) $t\bar{t}H$ leptonic, $H \to ZZ^* \to 4\ell$ $t\bar{t}H$ hadronic, $H \to ZZ^* \to 4\ell$			$t\bar{t}H$ 1 ℓ, boosted $t\bar{t}H$ 1 ℓ, resolved (11 categories) $t\bar{t}H$ 2 ℓ (7 categories)
VH	VH 2 ℓ VH 1 ℓ, $p_{\text{T}}^{\ell+E_{\text{T}}^{\text{miss}}} \geq 150$ GeV VH 1 ℓ, $p_{\text{T}}^{\ell+E_{\text{T}}^{\text{miss}}} < 150$ GeV VH $E_{\text{T}}^{\text{miss}}$, $E_{\text{T}}^{\text{miss}} \geq 150$ GeV VH $E_{\text{T}}^{\text{miss}}$, $E_{\text{T}}^{\text{miss}} < 150$ GeV VH+VBF $p_{\text{T}}^{j1} \geq 200$ GeV VH hadronic (2 categories)	VH leptonic 0-jet, $p_{\text{T}}^{4\ell} \geq 100$ GeV 2-jet, $m_{jj} < 120$ GeV			2 ℓ, $75 \leq p_{\text{T}}^{V} < 150$ GeV, $N_{\text{jets}} = 2$ 2 ℓ, $75 \leq p_{\text{T}}^{V} < 150$ GeV, $N_{\text{jets}} \geq 3$ 2 ℓ, $p_{\text{T}}^{V} \geq 150$ GeV, $N_{\text{jets}} = 2$ 2 ℓ, $p_{\text{T}}^{V} \geq 150$ GeV, $N_{\text{jets}} \geq 3$ 1 ℓ $p_{\text{T}}^{V} \geq 150$ GeV, $N_{\text{jets}} = 2$ 1 ℓ $p_{\text{T}}^{V} \geq 150$ GeV, $N_{\text{jets}} = 3$ 0 ℓ, $p_{\text{T}}^{V} \geq 150$ GeV, $N_{\text{jets}} = 2$ 0 ℓ, $p_{\text{T}}^{V} \geq 150$ GeV, $N_{\text{jets}} = 3$
VBF	VBF, $p_{\text{T}}^{\gamma\gamma jj} \geq 25$ GeV (2 categories) VBF, $p_{\text{T}}^{\gamma\gamma jj} < 25$ GeV (2 categories)	2-jet VBF, $p_{\text{T}}^{j1} \geq 200$ GeV 2-jet VBF, $p_{\text{T}}^{j1} < 200$ GeV	2-jet VBF	VBF $p_{\text{T}}^{\tau\tau} > 140$ GeV ($\tau_{\text{had}}\tau_{\text{had}}$ only) VBF high-m_{jj} VBF low-m_{jj}	
ggF	2-jet, $p_{\text{T}}^{\gamma\gamma} \geq 200$ GeV 2-jet, 120 GeV$\leq p_{\text{T}}^{\gamma\gamma} < 200$ GeV 2-jet, 60 GeV$\leq p_{\text{T}}^{\gamma\gamma} < 120$ GeV 2-jet, $p_{\text{T}}^{\gamma\gamma} < 60$ GeV 1-jet, $p_{\text{T}}^{\gamma\gamma} \geq 200$ GeV 1-jet, 120 GeV$\leq p_{\text{T}}^{\gamma\gamma} < 200$ GeV 1-jet, 60 GeV$\leq p_{\text{T}}^{\gamma\gamma} < 120$ GeV 1-jet, $p_{\text{T}}^{\gamma\gamma} < 60$ GeV 0-jet (2 categories)	1-jet, $p_{\text{T}}^{4\ell} \geq 120$ GeV 1-jet, 60 GeV$\leq p_{\text{T}}^{4\ell} < 120$ GeV 1-jet, $p_{\text{T}}^{4\ell} < 60$ GeV 0-jet, $p_{\text{T}}^{4\ell} < 100$ GeV	1-jet, $m_{\ell\ell} < 30$ GeV, $p_{\text{T}}^{\ell_2} < 20$ GeV 1-jet, $m_{\ell\ell} < 30$ GeV, $p_{\text{T}}^{\ell_2} \geq 20$ GeV 1-jet, $m_{\ell\ell} \geq 30$ GeV, $p_{\text{T}}^{\ell_2} < 20$ GeV 1-jet, $m_{\ell\ell} \geq 30$ GeV, $p_{\text{T}}^{\ell_2} \geq 20$ GeV 0-jet, $m_{\ell\ell} < 30$ GeV, $p_{\text{T}}^{\ell_2} < 20$ GeV 0-jet, $m_{\ell\ell} < 30$ GeV, $p_{\text{T}}^{\ell_2} \geq 20$ GeV 0-jet, $m_{\ell\ell} \geq 30$ GeV, $p_{\text{T}}^{\ell_2} < 20$ GeV 0-jet, $m_{\ell\ell} \geq 30$ GeV, $p_{\text{T}}^{\ell_2} \geq 20$ GeV	Boosted, $p_{\text{T}}^{\tau\tau} > 140$ GeV Boosted, $p_{\text{T}}^{\tau\tau} \leq 140$ GeV	

production mode	ggF	VBF	ZH	WH	$t\bar{t}H$
$C_1^i \times 100$	0.66	0.63	1.19	1.03	3.52
K_{EW}^i	1.049	0.932	0.947	0.93	1.014
κ_i^2	κ_F^2	κ_V^2	κ_V^2	κ_V^2	κ_F^2

Table 3: Values of C_1^i, K_{EW}^i and expression of κ_i^2 for each Higgs boson production process [9].

3 Theoretical model

Following Refs. [8, 9], in the present work the trilinear Higgs boson self coupling scales with κ_λ and the dependence of the Higgs boson production cross-sections on κ_λ is described by the relation:

$$\mu_i(\kappa_\lambda, \kappa_i) = \frac{\sigma^{\text{BSM}}}{\sigma^{\text{SM}}} = Z_H^{\text{BSM}}(\kappa_\lambda)\left[\kappa_i^2 + \frac{(\kappa_\lambda - 1)C_1^i}{K_{\text{EW}}^i}\right], \tag{2}$$

where $Z_H^{\text{BSM}}(\kappa_\lambda)$ is defined as:

$$Z_H^{\text{BSM}}(\kappa_\lambda) = \frac{1}{1 - (\kappa_\lambda^2 - 1)\delta Z_H} \quad \text{with} \quad \delta Z_H = -1.536 \times 10^{-3}, \tag{3}$$

$K_{\text{EW}}^i = \frac{\sigma_{\text{NLO}}^{\text{SM,i}}}{\sigma_{\text{LO}}^{\text{SM,i}}}$ accounts for the complete NLO EW correction of the production cross section for the process i in the SM hypothesis (*i.e.* $\kappa_\lambda = 1$), C_1^i is a process and kinematics-dependent linear coefficient that provides the sensitivity of the measurement to κ_λ, and $\kappa_i^2 = \frac{\sigma_{\text{LO,i}}^{\text{BSM}}}{\sigma_{\text{LO,i}}^{\text{SM}}}(\kappa_\lambda = 1)$ represents multiplicative modifiers to other Higgs boson couplings, parametrised as in the LO κ-framework [29]. In this work, only two coupling modifiers κ_F and κ_V are considered. They describe the modifications of the SM Higgs boson coupling to fermions and to massive vector bosons, respectively. As discussed in Ref. [9], for small deviations of κ_F and κ_V from 1, the dependence of NLO EW corrections on these coupling modifiers can be neglected. The values of these quantities for ggF, VBF, ZH, WH and $t\bar{t}H$ production modes are shown in Table 3, where the values of C_1^i and K_{EW}^i are averaged over the full phase space of these processes.

The variation of the trilinear coupling λ_{HHH} affects also the Higgs boson decay rates. Indicating with f a Higgs boson decay final state, the SM branching fraction is modified by the coefficient [9]:

$$\mu_f(\kappa_\lambda, \kappa_f) = \frac{\text{BR}_f^{\text{BSM}}}{\text{BR}_f^{SM}} = \frac{\kappa_f^2 + (\kappa_\lambda - 1)C_1^f}{\sum_j \text{BR}_j^{\text{SM}}\left[\kappa_j^2 + (\kappa_\lambda - 1)C_1^j\right]}. \tag{4}$$

where $\sum_j$ runs over all the Higgs boson decay channels, BR_j^{SM} is the Higgs boson SM decay rate to the j final state, κ_j is the branching fraction modifier for the j final state $\left(\kappa_j^2 = \text{BR}_{\text{LO};j}^{\text{BSM}}/\text{BR}_{\text{LO};j}^{\text{SM}}\right)$ that, as for the cross-section modifiers, is parametrised as function of κ_F and κ_V, and C_1^f is the coefficient that provides the NLO EW dependence on κ_λ. The values of C_1^f and the expressions of κ_f^2 are reported in Table 4 for all the

decay mode	$H \to \gamma\gamma$	$H \to WW^*$	$H \to ZZ^*$	$H \to b\bar{b}$	$H \to \tau\tau$
$C_1^f \times 100$	0.49	0.73	0.82	0	0
κ_f^2	$1.59\kappa_V^2 + 0.07\kappa_F^2 - 0.67\kappa_V\kappa_F$	κ_V^2	κ_V^2	κ_F^2	κ_F^2

Table 4: Values of C_1^f and expression of κ_f^2 for each considered Higgs boson decay mode [8, 9].

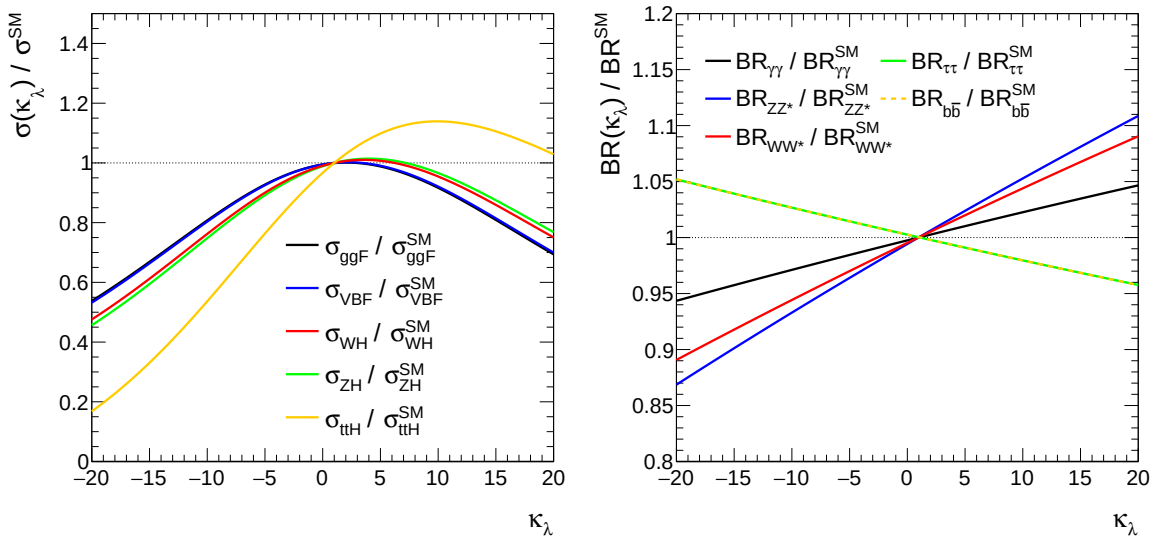

(a) (b)

Figure 2: Variation of the cross-sections (a) and branching fractions (b) as a function of the trilinear coupling modifier κ_λ. The plots represent the equations (2) and (4) using the numerical values shown in Tables 3 and 4, all obtained from Ref. [8, 9].

analysed decay modes. For Higgs bosons decaying into two fermions, the C_1^f coefficient is zero. The model under discussion, as shown in Eq. 2 and Eq. 4, does not include any additional contributions from new physics to the total width of the Higgs boson, or in the $gg \to H$ and $H \to \gamma\gamma$ loop mediated processes.

The dependence on κ_λ of the Higgs boson production cross sections and the decay branching fractions are shown in Figure 2.

3.1 Inclusion of event kinematic information

In the presence of a varied Higgs trilinear coupling, changes in κ_λ affect not only the inclusive rates of Higgs boson production and decay processes, but also their kinematics. In particular the largest deviations in kinematic distributions with respect to the to the SM are expected in the ZH, WH, and $t\bar{t}H$ production modes. On the contrary, in Higgs boson decay kinematics no significant modification are expected. Since the Higgs boson decays to two bodies in all decay channels, and it has a null spin, the angular distribution of the decay particles cannot be affected by BSM effects, being fully determined by the energy-momentum conservation and by the rotational symmetry of the decay. One exception is the decay to four fermions, that

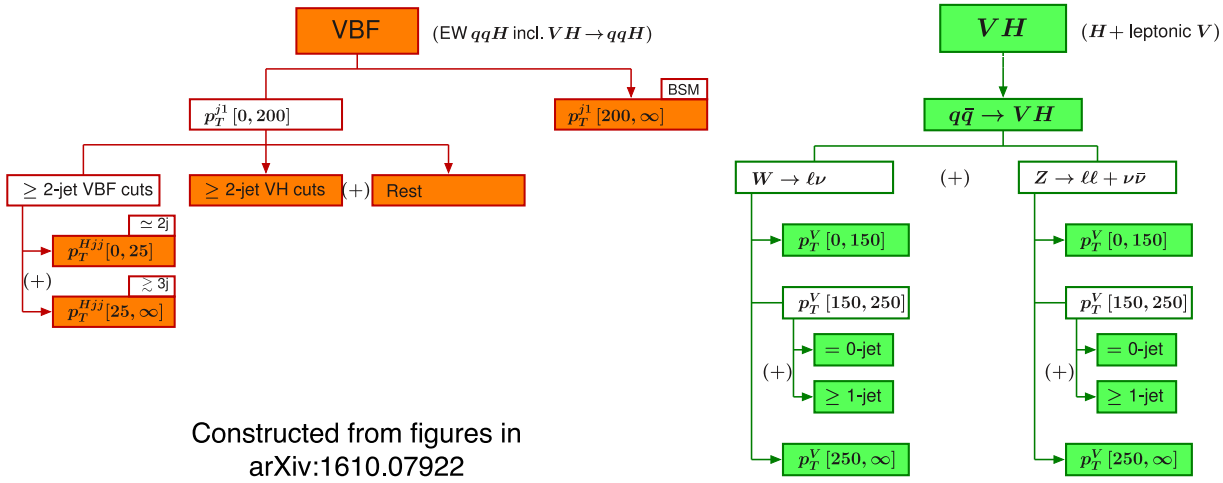

Figure 3: Schematic diagram of the VBF + V(had)H (left) and V(lep)H (right) STXS regions. p_{T}^{Hjj} is the p_{T} of the Higgs boson plus two jets system, p_{T}^{V} is the p_{T} of the vector boson V in the VH production mode, p_{T}^{j1} is the p_{T} of the jet with the highest p_{T}. In the VH, $H \to b\bar{b}$ analysis, the separation in jet number of the p_{T}^{V} [150, 250] region in the VH production mode has been ignored, merging the 0 and the ≥ 1 jet regions. The diagrams are obtained from Ref. [14].

is typically mediated by the WW^* and ZZ^* vector boson state. Also in this case, due to the extremely small coupling of the Higgs boson to electrons and muons, differential contributions from κ_λ are negligible [9].

The dependence of the κ_λ corrections on kinematics can be partially taken into account by exploiting cross-section measurements in regions defined by the STXS stage-1 framework. In this work, this has been done for the VBF, ZH and WH production modes, for which the STXS phase space region definitions are shown in Figure 3. The STXS region choice is not a priori optimized to constrain κ_λ, but the granularity of the stage-1 configuration allows to apply the κ_λ model in smaller kinematic regions, with respect to the inclusive phase space. The advantage of a more differential description of the dependence on κ_λ is, on one hand, to reduce the potential bias on the determination of κ_λ introduced by the analysis efficiency and sensitivity being dependent on kinematics, and on the other hand, to exploit such kinematic dependence to further increase the sensitivity to κ_λ.

For ggF production, differential κ_λ corrections are not yet available, because these involve higher order calculations including two loop corrections. Therefore STXS regions related to ggF share the same parametrization as for the inclusive ggF production. Since no differential measurement in terms of STXS regions is available in the input channels for the $t\bar{t}H$ production mode, only the inclusive cross-section dependence on κ_λ has been considered in this case. The $gg \to ZH$ cross-section is not parametrised as a function of κ_λ, because the theoretical computation is still missing. Present data are not sensitive to this production mode; moreover, it should contribute mostly in high p_{T}^{H} regions where the sensitivity to κ_λ is expected to be small. Finally, the $b\bar{b}H$ and single top associated Higgs boson production modes are not parametrised as a function of κ_λ. However, they contribute, together with the $gg \to ZH$ production mode, to constrain κ_F and κ_V, when these modifiers are fitted simultaneously with κ_λ. On the contrary, their cross-sections are fixed to the SM value, when fitting κ_λ only.

The parametrization of the variation of the production cross-section as a function of κ_λ contained in Eq. 2, can be adapted to describe the cross-section in each single STXS region. This requires re-deriving the value of the kinematic dependent coefficients C_1^i in each region defined in the measurement. For each VBF, ZH,

STXS region		VBF	WH	ZH
		$C_1^i \times 100$		
$VBF + V(had)H$	VBF-cuts + $p_T^{j1} < 200$ GeV, $\leq 2j$	0.63	0.91	1.07
	VBF-cuts + $p_T^{j1} < 200$ GeV, $\geq 3j$	0.61	0.85	1.04
	VH-cuts + $p_T^{j1} < 200$ GeV	0.64	0.89	1.10
	no VBF/VH-cuts, $p_T^{j1} < 200$ GeV	0.65	1.13	1.28
	$p_T^{j1} > 200$ GeV	0.39	0.23	0.28
$qq \to H\ell\nu$	$p_T^V < 150$ GeV		1.15	
	$150 < p_T^V < 250$ GeV, $0j$		0.18	
	$150 < p_T^V < 250$ GeV, $\geq 1j$		0.33	
	$p_T^V > 250$ GeV		0	
$qq \to H\ell\ell$	$p_T^V < 150$ GeV			1.33
	$150 < p_T^V < 250$ GeV, $0j$			0.20
$qq \to H\nu\nu$	$150 < p_T^V < 250$ GeV, $\geq 1j$			0.39
	$p_T^V > 250$ GeV			0

Table 5: C_1^i coefficients for each region of the STXS scheme for the VBF, WH and ZH production modes. The same definition for STXS regions and production modes as in Table 2 is used. In the VBF categories, "VBF-cuts" [14] indicates selections applied to target the VBF di-jet topology, with requirements on the di-jet invariant mass (m_{jj}) and the difference in pseudorapidity between the two jets; the additional $\leq 2j$ and $\geq 3j$ region separation is performed indirectly by requesting $p_T^{Hjj} \lesssim 25$ GeV. "VH-cuts" select the $W, Z \to jj$ decays, requiring an m_{jj} value close to the vector boson mass [14]. The C_1^i coefficients of the $p_T^V > 250$ GeV regions are negligible, $O(10^{-6})$, and are set to 0.

WH region of the STXS stage-1 framework, the C_1^i coefficient has been computed using samples of events generated at LO EW using MadGraph5_aMC@NLO 2.5.5 [30], and reweighted on an event-by-event basis with the tool provided in Ref. [31]. This tool evaluates the self coupling dependent contribution of the NLO EW correction, selecting only the relevant one-loop diagrams that include trilinear Higgs boson vertices, but not self energy insertions. For each region i of the STXS framework, C_1^i is defined as the relative difference between the number of reweighted NLO events and LO events [9]. The C_1^i values are reported in Table 5. The total electroweak corrections represented by the coefficients K_{EW}^i and entering in Eq. 2 also depend on the event kinematics. However, in the regions of phase space where these corrections are most significant (typically for high Higgs boson transverse momentum), the sensitivity to the Higgs boson trilinear coupling is minimal [9]. For example for the WH and ZH production modes, K_{EW}^i variations of approximately 15% with respect to the inclusive value are expected only in high p_T^H regions, where the κ_λ sensitivity is suppressed ($C_1^i \simeq 0$ in high p_T^H regions). For this reason, the coefficients K_{EW}^i can be assumed to be constant to a good approximation and set to their inclusive values that were already reported in Table 3.

Due to the variations of the kinematic distributions, the selection efficiency of the input analyses can also depend on κ_λ. This effect has been tested using Monte Carlo samples, generated at LO with MadGraph5_aMC@NLO 2.5.5 and reweighted with a λ_{HHH}-dependent NLO EW correction for different values of κ_λ. In general, a negligible dependence is found, except for the $t\bar{t}H$ production, which is characterized by a stronger κ_λ kinematic dependence: the selection efficiency in the $H \to \gamma\gamma$ analysis increases by 10% for $\kappa_\lambda < -10$, but in this interval the reduction of the cross-section due to the κ_λ

dependence is about 80% with respect to the nominal, therefore largely dominating over the efficiency variation. For this reason, the selection efficiencies can be reasonably assumed to be constant as a function of κ_λ, and this assumption is made in the analysis presented here. However, this assumption will need to be re-evaluated also in the ggF production mode once a complete computation of the differential NLO EW corrections become available.

4 Statistical model

The statistical treatment used in this note follows the procedures described in Refs. [3, 4] . The result of the combination is obtained from a likelihood function $L(\boldsymbol{\alpha}, \boldsymbol{\theta})$, where $\boldsymbol{\alpha}$ represents the vector of the parameters of interest (POI) of the model and $\boldsymbol{\theta}$ is the set of nuisance parameters, which includes the systematic uncertainty contributions and background parameters that are constrained by side bands or control regions in data. The global likelihood function $L(\boldsymbol{\alpha}, \boldsymbol{\theta})$ is obtained as the product of the likelihoods of the input analyses. These are themselves products of likelihoods computed in the mutually orthogonal categories optimised in each analysis.

The number of signal events in each analysis category j is defined as:

$$n_j^{\text{signal}}(\kappa_\lambda, \kappa_F, \kappa_V, \boldsymbol{\theta}) = \mathcal{L}_j(\boldsymbol{\theta}) \sum_i \sum_f \mu_{if}(\kappa_\lambda, \kappa_F, \kappa_V)(\sigma_{\text{SM},i}(\boldsymbol{\theta}) \times \text{BR}_{\text{SM},f}(\boldsymbol{\theta}))(\epsilon \times A)_{if,j}(\boldsymbol{\theta}), \tag{5}$$

where the index i runs over all the production regions defined by the STXS stage-1 framework and the index f includes all the considered decay channels, *i.e.* $f = \gamma\gamma, ZZ^*, WW^*, \tau\tau, b\bar{b}$. $\mathcal{L}_j$, is the integrated luminosity of the dataset used in the j category, and $(\epsilon \times A)_{if,j}$ represents the acceptance and efficiency estimation for the category j, production process i and decay channel f. All these terms depend also on a set of nuisance parameters $\boldsymbol{\theta}$, that account for the theoretical and systematic uncertainties that can affect the luminosity, the cross-section and branching fraction prediction, the efficiency estimation, and the background estimation. For a complete discussion of these and other sources of systematic uncertainty please refer to the individual analysis papers referenced in Table 1. Finally, $\mu_{if}(\kappa_\lambda, \kappa_F, \kappa_V) = \mu_i(\kappa_\lambda, \kappa_F, \kappa_V) \times \mu_f(\kappa_\lambda, \kappa_F, \kappa_V)$, where μ_i is defined in Eq. 2 and μ_f in Eq. 4, describes the yield dependence on the Higgs boson self-coupling modifier κ_λ, and on the single Higgs boson coupling modifiers κ_V and κ_F, representing potential deviations from the SM expectation.

Confidence intervals for the POIs are determined using the profile likelihood ratio [32] as test statistics:

$$\Lambda(\boldsymbol{\alpha}) = \frac{L(\boldsymbol{\alpha}, \hat{\hat{\boldsymbol{\theta}}}(\boldsymbol{\alpha}))}{L(\hat{\boldsymbol{\alpha}}, \hat{\boldsymbol{\theta}})}. \tag{6}$$

In the numerator the nuisance parameters are set to their *profiled* values $\hat{\hat{\boldsymbol{\theta}}}(\boldsymbol{\alpha})$, that maximise the likelihood for a given set of values of $\boldsymbol{\alpha}$. In the denominator both the parameters of interest and the nuisance parameters are respectively set to the values $\hat{\boldsymbol{\alpha}}$ and $\hat{\boldsymbol{\theta}}$, that simultaneously maximise the likelihood $L(\boldsymbol{\alpha}, \boldsymbol{\theta})$. In the asymptotic regime, $-2 \log \Lambda(\boldsymbol{\alpha}, \boldsymbol{\theta})$ is approximately distributed as a χ^2 statistic with n degrees of freedom, where n equals the number of parameters of interests in the model. The results presented in this note are based on the profile-likelihood evaluation, and 68% as well as 95% C.L. intervals are given in the asymptotic approximation [32].

In some case the results in the note are presented with the uncertainty decomposed in separate contributions: theoretical uncertainties affecting the background processes, theoretical uncertainties affecting the Higgs boson signal, experimental uncertainties and statistical uncertainties. The values of the uncertainty components are derived by fixing the related nuisance parameters to their best value $\hat{\theta}$ in the numerator and the denominator of Λ. This procedure is repeated sequentially for each source of uncertainty following the same order in which they are listed above. The value of each component is then evaluated as the quadratic difference between the resulting uncertainty at each step and the uncertainty obtained in the previous one, where for the initial step the total uncertainty is considered. The statistical uncertainty is then evaluated at the last step, fixing all the nuisance parameters except to the ones that are only constrained by data, such as the data-driven background normalization.

5 Results

5.1 Result of fits to κ_λ

In this section, the main result of this analysis is presented, where a likelihood fit is performed to constrain the value of the Higgs boson self-coupling κ_λ, while leaving untouched all other Higgs boson couplings ($\kappa_V = \kappa_F = 1$). A large variety of models beyond the SM exists where new physics is expected to only appear in a modification of the Higgs boson self-coupling, as for example the Higgs-boson portal models in the alignment limit [33]. In these BSM scenarios, the constraints on κ_λ, derived through the combination of single-Higgs measurements, can be directly compared to the constraints set by double Higgs production measurements.

The κ_λ self-coupling modifier is probed in the range $-20 < \kappa_\lambda < 20$, because outside this range the calculation in Ref. [8] loses its validity.

The value of $-2\ln\Lambda(\kappa_\lambda)$ as a function of κ_λ is shown in Figure 4 for the data and the Asimov dataset [32], generated from the likelihood distribution Λ with nuisance parameters fixed at the best fit value obtained on data and the parameter of interest fixed to SM hypothesis (*i.e.* $\kappa_\lambda = 1$). The central value and uncertainty of the κ_λ modifier of the trilinear Higgs boson self-coupling is determined to be:

$$\kappa_\lambda = 4.0^{+4.3}_{-4.1} = 4.0^{+3.7}_{-3.6}\,(\text{stat.})\,^{+1.6}_{-1.5}\,(\text{exp.})\,^{+1.3}_{-0.9}\,(\text{sig. th.})\,^{+0.8}_{-0.9}\,(\text{bkg. th.}),$$

where the total uncertainty is decomposed into components for statistical uncertainties, experimental systematic uncertainties, and theory uncertainties on signal and background modelling, following the procedure described in Section 4. The 95% C.L. interval of κ_λ is $-3.2 < \kappa_\lambda < 11.9$ (observed) and $-6.2 < \kappa_\lambda < 14.4$ (expected). This interval is comparable to the one obtained from the direct HH searches using an integrated luminosity of 36.1 fb^{-1}[6], which is $-5.0 < \kappa_\lambda < 12.1$ (observed) and $-5.8 < \kappa_\lambda < 12.0$ (expected).

The difference in the shape of the likelihood curves in Figure 4 between the Asimov sample and the data is due to the non-linearity of the cross-section dependence from κ_λ and the difference of the best-fit values of κ_λ in the two cases. As shown by Figure 2, the sensitivity to κ_λ is not constant. The likelihood shape is affected by the different behaviour of the quadratic and linear κ_λ dependent terms: for example, if κ_λ is < 1 both terms induce a reduction of the Higgs boson production cross-sections, while for $\kappa_\lambda > 1$ there are larger cancellations that weaken the cross-section dependence on κ_λ [9]. Moreover, the global likelihood shape depends on combining the contributions from the different production and decay modes, which all have different sensitivities and in most cases also significantly different likelihood shapes, as shown in

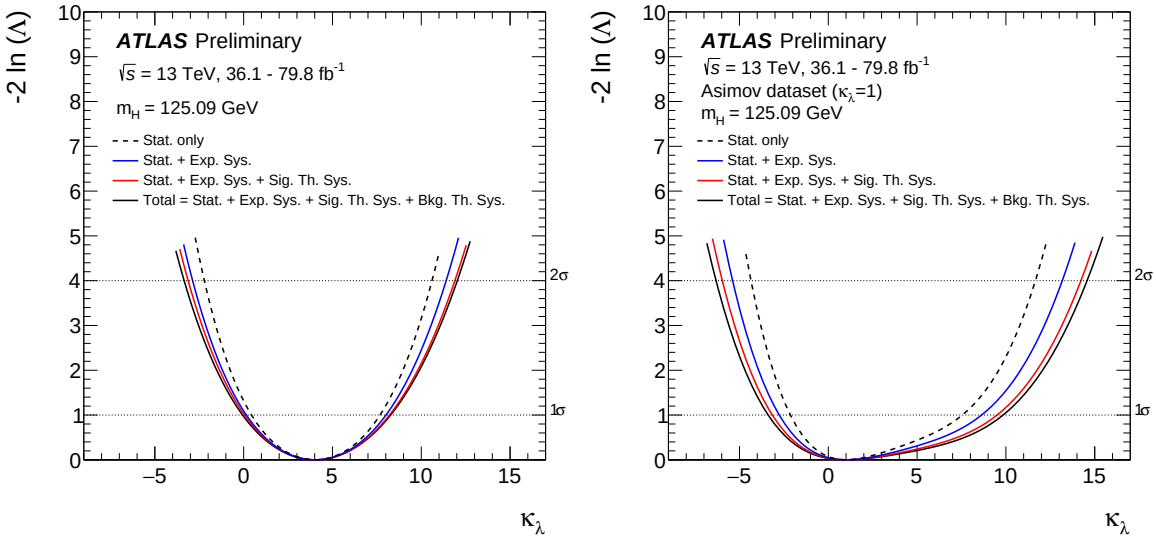

Figure 4: Profile likelihood scan, in terms of $-2\ln\Lambda(\kappa_\lambda)$, performed as a function of κ_λ on data (a) and on the Asimov dataset [32] generated under the SM hypothesis (b). The solid black line shows the profile likelihood distributions obtained including all systematic uncertainties ("Total"). Results from a statistic only fit "Stat. only" (black dashed line), including the experimental systematics "Stat. + Exp. Sys." (blue solid line) , adding theory systematics related to the signal "Stat.+ Exp. Sys.+ Sig. Th. Sys." (red solid line) are also shown. The dotted horizontal lines show the $-2\ln\Lambda(\kappa_\lambda) = 1$ and $-2\ln\Lambda(\kappa_\lambda) = 4$ levels that are used to define the $\pm1\sigma$ and $\pm2\sigma$ uncertainties on κ_λ.

Figure 5. The dominant contributions to the κ_λ sensitivity derive from the di-boson decay channels $\gamma\gamma$, ZZ^*, WW^* and from the ggF and $t\bar{t}H$ production modes.

The production mode that is most sensitive to the Higgs boson self-coupling is gluon fusion. In order to cross-check the effect on the results from assuming a kinematic independent parametrization of the gluon fusion production cross-section as a function of κ_λ, an additional fit has been performed by excluding the STXS bins with Higgs boson transverse momentum above 120 GeV. This has been technically realized by introducing signal strength parameters for these STXS bins and profiling them independently in the fit. The result is a minimal change of the central value ($\sim 5\%$) and uncertainty on κ_λ.
In addition, the impact on the κ_λ determination of using an inclusive cross-section measurement, rather than the differential cross-section information contained in the STXS bins, has been studied. An alternative fit has been performed where the VBF, VH and ZH production modes are considered as single inclusive bins. Compared to the use of differential information, the inclusive fit does not currently lead to a significant loss in sensitivity to κ_λ. However, differential information should help most in the $t\bar{t}H$ production mode, where it is currently not considered. All results are summarised in Table 6.

5.2 Results of fits to κ_λ and either κ_V or κ_F

Two additional fit configurations are considered in this note, in which a simultaneous fit is performed to κ_λ and κ_F, or to κ_λ and κ_V. The remaining coupling modifier that is not included in the fit, κ_V in the first case and κ_F in the second case, is kept fixed to the SM prediction. These fits target BSM scenarios where new

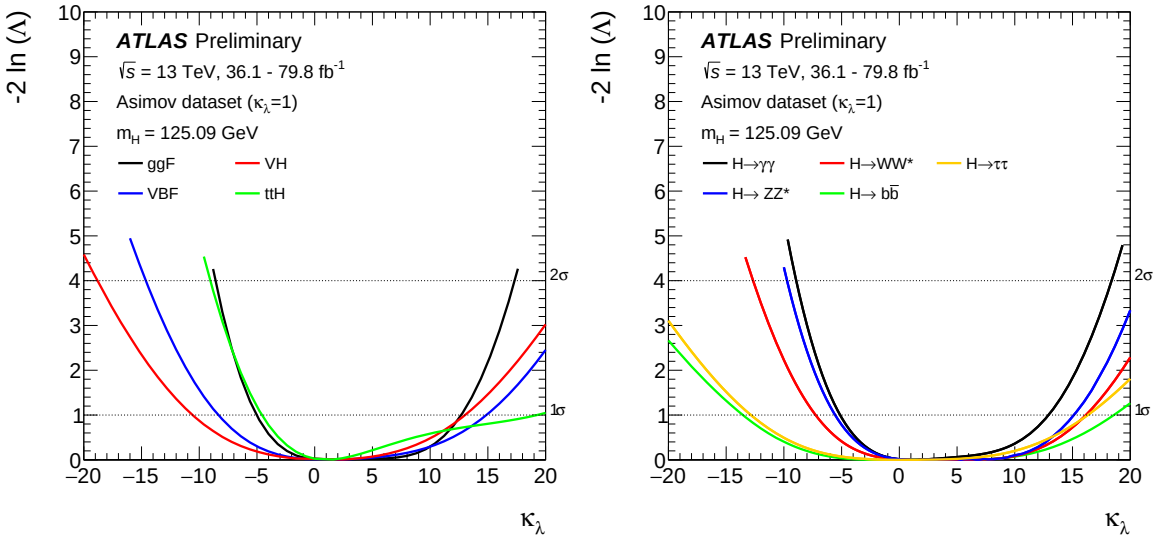

Figure 5: Profile likelihood scan, in terms of $-2\ln\Lambda(\kappa_\lambda)$, performed as a function of κ_λ on Asimov datasets [32] generated under the SM hypothesis for each Higgs boson production mode (a) and each decay channel (b). In (a) the scan is performed parametrising all branching fractions and the selected production mode cross-section as a function of κ_λ, while fixing the cross-section of the other production modes at the SM value, in (b) all production mode cross-sections and decay branching fractions are expressed as a function of κ_λ, but only the categories of the selected channel are included in the fit. The $t\bar{t}H$ multi-lepton categories are excluded from the $H \to ZZ^*$, $H \to WW^*$, and $H \to \tau\tau$ fits.

physics could affect only the Yukawa type terms ($\kappa_V = 1$) of the SM or only the couplings to vector bosons ($\kappa_F = 1$), in addition to the Higgs boson self-coupling (κ_λ) [34].

The theory parametrization used in this study in terms of cross section dependence on κ_λ and κ_V or κ_F assumes partial factorization of the changes to the cross section induced by the single-Higgs coupling modifiers κ_V, κ_F, and those induced by the self-coupling modifier κ_λ. While this assumption is not justified in the presence of large deviations from the SM expectations, it also reflects the fact that NLO EW correction are not theoretically well defined after introducing LO-motivated single-Higgs coupling modifiers. While a more complete theoretical framework (such as an Effective Field Theory approach) is needed to overcome these difficulties, the results presented in this section give a rough indication of the simultaneous sensitivity to both Higgs boson self-coupling and single Higgs boson couplings with the data statistics currently available for the input analyses. The results are summarised in Table 6.

Figure 6 shows negative log-likelihood contours on the $(\kappa_\lambda, \kappa_F)$ and $(\kappa_\lambda, \kappa_V)$ grids obtained from fits performed in the $\kappa_V = 1$ or $\kappa_F = 1$ hypothesis, respectively. As expected, including additional degrees of freedom to the fit reduces the constraining power of the measurement. In particular, the sensitivity to κ_λ is not much degraded when determining κ_F at the same time, while it is degraded by 50% (on the expected lower 95% C.L. exclusion limit) when determining simultaneously κ_V and κ_λ. An even less constrained fit, performed by either fitting simultaneously κ_λ, κ_V and κ_F, or fitting simultaneously κ_λ and a common single Higgs boson coupling modifier ($\kappa = \kappa_V = \kappa_F$), results in nearly no sensitivity to κ_λ within the theoretically allowed range of $|\kappa_\lambda| < 20$.

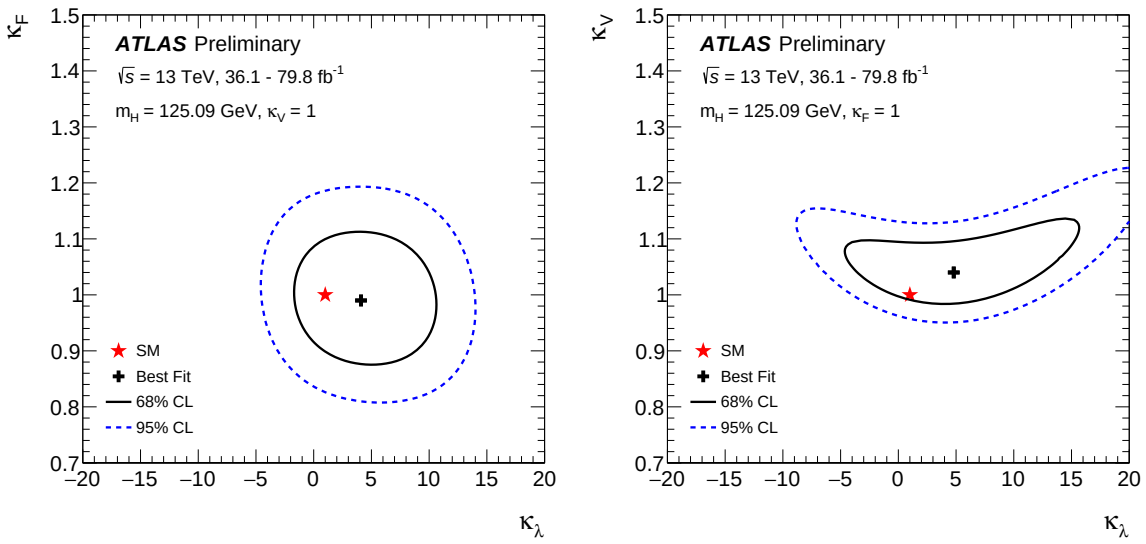

(a) (b)

Figure 6: Negative log-likelihood contours at 68% and 95% C.L. in the $(\kappa_\lambda, \kappa_F)$ plane under the assumption of $\kappa_V = 1$ (a), and in the $(\kappa_\lambda, \kappa_V)$ plane under the assumption of $\kappa_F = 1$ (b). The best fit value is indicated by a cross while the SM hypothesis is indicated by a star. The plot assumes that the approximations in Refs. [8,9] are valid inside the shown contours.

6 Conclusion

The Higgs boson self-coupling modifier $\kappa_\lambda = \lambda_{HHH}/\lambda^{SM}_{HHH}$ has been extracted with a global fit procedure [8, 9] applied to the combination of analyses targeting the single Higgs production modes on data collected at $\sqrt{s} = 13$ TeV up to an integrated luminosity of up to 80 fb^{-1} [4]. In the simplified assumption that all deviations from the SM expectation have to be interpreted as a modification of the trilinear coupling of the Higgs boson, the best fit value of κ_λ is $\kappa_\lambda = 4.0^{+4.3}_{-4.1}$, excluding at the 95% C.L. values outside the interval $-3.2 < \kappa_\lambda < 11.9$. Additional results, including the simultaneous determination of the Higgs boson self-coupling and single Higgs boson couplings to either fermions or bosons, have also been derived.

This analysis shows that an alternative and complementary approach to constrain the Higgs boson self-coupling through direct double Higgs production searches is feasible. This approach can provide sensitivity that is not far from to the more direct determination of the Higgs boson self-coupling through double Higgs production. However, the constraints become significantly weaker in new physics scenarios where simultaneous modifications to the single Higgs boson couplings are allowed, to the point of almost vanishing when a single overall Higgs coupling rescaling modifier is considered. The differential information currently provided by the STXS regions in the VBF, WH and ZH production modes does not help to remove such degeneracies nor to improve the sensitivity to κ_λ significantly. Nevertheless, a dedicated optimization of the kinematic binning, including the most sensitive ggF and $t\bar{t}H$ production modes, still needs to be fully theoretically and experimentally explored and might improve the sensitivity in the future.

POIs	Granularity	$\kappa_F{}^{+1\sigma}_{-1\sigma}$	$\kappa_V{}^{+1\sigma}_{-1\sigma}$	$\kappa_\lambda{}^{+1\sigma}_{-1\sigma}$	κ_λ [95% C.L.]
κ_λ	STXS	1	1	$4.0^{+4.3}_{-4.1}$	$[-3.2, 11.9]$
				$1.0^{+8.8}_{-4.4}$	$[-6.2, 14.4]$
κ_λ	inclusive	1	1	$4.6^{+4.3}_{-4.2}$	$[-2.9, 12.5]$
				$1.0^{+9.5}_{-4.3}$	$[-6.1, 15.0]$
κ_λ, κ_V	STXS	1	$1.04^{+0.05}_{-0.04}$	$4.8^{+7.4}_{-6.7}$	$[-6.7, 18.4]$
			$1.00^{+0.05}_{-0.04}$	$1.0^{+9.9}_{-6.1}$	$[-9.4, 18.9]$
κ_λ, κ_F	STXS	$0.99^{+0.08}_{-0.08}$	1	$4.1^{+4.3}_{-4.1}$	$[-3.2, 11.9]$
		$1.00^{+0.08}_{-0.08}$		$1.0^{+8.8}_{-4.4}$	$[-6.3, 14.4]$

Table 6: Best fit values for κ modifiers with $\pm1\sigma$ uncertainties. The first column shows the parameter(s) of interest in each fit configuration, where the other coupling modifiers are kept fixed to the SM prediction. The fit to determine κ_λ has been performed in two configurations, one using the full STXS granularity for VBF, ZH and WH (STXS), and the other only considering the inclusive parametrization for all the production modes (inclusive). The 95% C.L. interval for κ_λ is also reported. For each fit result the upper row corresponds to the observed results, and the lower row to the expected results obtained using Asimov datasets generated under the SM hypothesis [32]. The κ_λ, κ_V and κ_λ, κ_F fit results are obtained under the assumption that the approximations in Refs. [8,9] are valid in 95% C.L. regions.

References

[1] ATLAS Collaboration, *Observation of a new particle in the search for the Standard Model Higgs boson with the ATLAS detector at the LHC*, Phys. Lett. B **716** (2012) 1, arXiv: 1207.7214 [hep-ex].

[2] CMS Collaboration, *Observation of a new boson at a mass of 125 GeV with the CMS experiment at the LHC*, Phys. Lett. B **716** (2012) 30, arXiv: 1207.7235 [hep-ex].

[3] ATLAS and CMS Collaborations, *Measurements of the Higgs boson production and decay rates and constraints on its couplings from a combined ATLAS and CMS analysis of the LHC pp collision data at* $\sqrt{s} = 7$ *and* 8 *TeV*, JHEP **08** (2016) 045, arXiv: 1606.02266 [hep-ex].

[4] ATLAS Collaboration, *Combined measurements of Higgs boson production and decay using up to* 80 fb^{-1} *of proton–proton collision data at* $\sqrt{s} = 13$ *TeV collected with the ATLAS experiment*, ATLAS-CONF-2019-005, 2019, URL: http://cds.cern.ch/record/2668375.

[5] CMS Collaboration, *Combined measurements of Higgs boson couplings in proton–proton collisions at* $\sqrt{s} = 13$ *TeV*, Eur. Phys. J. (2018), arXiv: 1809.10733 [hep-ex].

[6] ATLAS Collaboration, *Combination of searches for Higgs boson pairs in pp collisions at* 13 *TeV with the ATLAS experiment*, ATLAS-CONF-2018-043, 2018, URL: https://cds.cern.ch/record/2638212.

[7] CMS Collaboration, *Combination of searches for Higgs boson pair production in proton-proton collisions at* $\sqrt{s}$ = 13 TeV, CMS-PAS-HIG-17-030, 2018, URL: https://cds.cern.ch/record/2628486.

[8] G. Degrassi, P. P. Giardino, F. Maltoni and D. Pagani, *Probing the Higgs self coupling via single Higgs production at the LHC*, JHEP **12** (2016) 080, arXiv: 1607.04251 [hep-ph].

[9] F. Maltoni, D. Pagani, A. Shivaji and X. Zhao, *Trilinear Higgs coupling determination via single-Higgs differential measurements at the LHC*, Eur. Phys. J. **C77** (2017) 887, arXiv: 1709.08649 [hep-ph].

[10] S. Di Vita, C. Grojean, G. Panico, M. Riembau and T. Vantalon, *A global view on the Higgs self-coupling*, JHEP **09** (2017) 069, arXiv: 1704.01953 [hep-ph].

[11] M. Gorbahn and U. Haisch, *Indirect probes of the trilinear Higgs coupling:* $gg \to h$ *and* $h \to \gamma\gamma$, JHEP **10** (2016) 094, arXiv: 1607.03773 [hep-ph].

[12] W. Bizon, M. Gorbahn, U. Haisch and G. Zanderighi, *Constraints on the trilinear Higgs coupling from vector boson fusion and associated Higgs production at the LHC*, JHEP **07** (2017) 083, arXiv: 1610.05771 [hep-ph].

[13] M. McCullough, *An Indirect Model-Dependent Probe of the Higgs Self-Coupling*, Phys. Rev. **D90** (2014) 015001, [Erratum: Phys. Rev.D92,no.3,039903(2015)], arXiv: 1312.3322 [hep-ph].

[14] D. de Florian et al., *Handbook of LHC Higgs Cross Sections: 4. Deciphering the Nature of the Higgs Sector*, (2016), arXiv: 1610.07922 [hep-ph].

[15] J. R. Andersen et al., 'Les Houches 2015: Physics at TeV Colliders Standard Model Working Group Report', *9th Les Houches Workshop on Physics at TeV Colliders (PhysTeV 2015) Les Houches, France, June 1-19, 2015*, 2016, arXiv: 1605.04692 [hep-ph], URL: http://lss.fnal.gov/archive/2016/conf/fermilab-conf-16-175-ppd-t.pdf.

[16] ATLAS Collaboration, *Measurement of Higgs boson properties in the diphoton decay channel using* 80 fb^{-1} *of pp collision data at* $\sqrt{s}$ = 13 *TeV with the ATLAS detector*, ATLAS-CONF-2018-028, 2018, URL: https://cds.cern.ch/record/2628771.

[17] ATLAS Collaboration, *Measurements of Higgs boson properties in the diphoton decay channel with* 36 fb^{-1} *of pp collision data at* $\sqrt{s}$ = 13 *TeV with the ATLAS detector*, Phys. Rev. D **98** (2018) 052005, arXiv: 1802.04146 [hep-ex].

[18] ATLAS Collaboration, *Observation of Higgs boson production in association with a top quark pair at the LHC with the ATLAS detector*, Phys. Lett. B **784** (2018) 173, arXiv: 1806.00425 [hep-ex].

[19] ATLAS Collaboration, *Measurements of the Higgs boson production, fiducial and differential cross sections in the* 4ℓ *decay channel at* $\sqrt{s}$ = 13 *TeV with the ATLAS detector*, ATLAS-CONF-2018-018, 2018, URL: https://cds.cern.ch/record/2621479.

[20] ATLAS Collaboration, *Measurement of the Higgs boson coupling properties in the* $H \to ZZ^* \to 4\ell$ *decay channel at* $\sqrt{s}$ = 13 *TeV with the ATLAS detector*, JHEP **03** (2018) 095, arXiv: 1712.02304 [hep-ex].

[21] ATLAS Collaboration,
Observation of $H \to b\bar{b}$ decays and VH production with the ATLAS detector,
Phys. Lett. B **786** (2018) 59, arXiv: 1808.08238 [hep-ex].

[22] ATLAS Collaboration, *Measurements of VH, $H \to b\bar{b}$ production as a function of the vector boson transverse momentum in* 13 *TeV pp collisions with the ATLAS detector*, ATLAS-CONF-2018-053, 2018, URL: https://cds.cern.ch/record/2649082.

[23] ATLAS Collaboration,
Measurements of gluon-gluon fusion and vector-boson fusion Higgs boson production cross-sections in the $H \to WW^* \to e\nu\mu\nu$ decay channel in pp collisions at $\sqrt{s}$ = 13 TeV with the ATLAS detector, (2018), arXiv: 1808.09054 [hep-ex].

[24] ATLAS Collaboration, *Cross-section measurements of the Higgs boson decaying into a pair of τ-leptons in proton–proton collisions at $\sqrt{s}$ = 13 TeV with the ATLAS detector*, Phys. Rev. (2018), arXiv: 1811.08856 [hep-ex].

[25] ATLAS Collaboration, *Evidence for the associated production of the Higgs boson and a top quark pair with the ATLAS detector*, Phys. Rev. D **97** (2018) 072003, arXiv: 1712.08891 [hep-ex].

[26] ATLAS Collaboration, *Search for the standard model Higgs boson produced in association with top quarks and decaying into a $b\bar{b}$ pair in pp collisions at $\sqrt{s}$ = 13 TeV with the ATLAS detector*, Phys. Rev. D **97** (2018) 072016, arXiv: 1712.08895 [hep-ex].

[27] ATLAS Collaboration, *The ATLAS Experiment at the CERN Large Hadron Collider*,
JINST **3** (2008) S08003.

[28] ATLAS Collaboration, *ATLAS Insertable B-Layer Technical Design Report*, 2010,
URL: https://cds.cern.ch/record/1291633.

[29] LHC Higgs Cross Section Working Group, S. Heinemeyer, C. Mariotti, G. Passarino and R. Tanaka (Eds.), *Handbook of LHC Higgs Cross Sections: 3. Higgs Properties*,
CERN-2013-004 (CERN, Geneva, 2013), arXiv: 1307.1347 [hep-ph].

[30] J. Alwall et al., *The automated computation of tree-level and next-to-leading order differential cross sections, and their matching to parton shower simulations*, JHEP **07** (2014) 079,
arXiv: 1405.0301 [hep-ph].

[31] A. Shivaji and X. Zhao, *Higgs Trilinear self-coupling determination through one-loop effects*, 2017,
URL: https://cp3.irmp.ucl.ac.be/projects/madgraph/wiki/HiggsSelfCoupling.

[32] G. Cowan, K. Cranmer, E. Gross and O. Vitells,
Asymptotic formulae for likelihood-based tests of new physics,
Eur. Phys. J. **C71** (2011) 1554, [Erratum: Eur. Phys. J.C73,2501(2013)],
arXiv: 1007.1727 [physics.data-an].

[33] M. Carena, H. E. Haber, I. Low, N. R. Shah and C. E. M. Wagner,
Alignment limit of the NMSSM Higgs sector, Phys. Rev. **D93** (2016) 035013,
arXiv: 1510.09137 [hep-ph].

[34] M. B. Einhorn and J. Wudka, *Higgs-Boson Couplings Beyond the Standard Model*,
Nucl. Phys. **B877** (2013) 792, arXiv: 1308.2255 [hep-ph].